Monthly Notices
of the
ROYAL ASTRONOMICAL SOCIETY

MNRAS **482,** 175–183 (2019)
Advance Access publication 2018 September 21

doi:10.1093/mnras/sty2605

Timing analysis and pulse profile of the Vela pulsar in the optical band from Iqueye observations

A. Spolon,[1] L. Zampieri,[2★] A. Burtovoi,[2] G. Naletto,[1,2] C. Barbieri,[1,2] M. Barbieri,[3] A. Patruno[4,5] and E. Verroi[6]

[1]*Department of Physics and Astronomy 'G. Galilei', University of Padova, Via Marzolo, 8, I-35131 Padova, Italy*
[2]*INAF – Astronomical Observatory of Padova, Vicolo dell' Osservatorio 5, I-35122 Padova, Italy*
[3]*Department of Physics, University of Atacama, Copayapu 485, Copiapo, Chile*
[4]*Leiden Observatory, Leiden University, Neils Bohrweg 2, NL-2333 CA Leiden, the Netherlands*
[5]*ASTRON, the Netherlands Institute for Radio Astronomy, Postbus 2, NL-7900 AA Dwingeloo, the Netherlands*
[6]*TIFPA – Trento Institute for Fundamentals Physics Applications, Via Sommarive 14, I-38123 Povo, Italy*

Accepted 2018 September 14. Received 2018 September 4; in original form 2018 April 3

ABSTRACT

The Vela pulsar is among a number of pulsars which show detectable optical pulsations. We performed optical observations of this pulsar in 2009 January and December with the Iqueye instrument mounted at the ESO 3.5 m New Technology Telescope. Our aim was to perform phase fitting of the Iqueye data, and to measure the optical pulse profile of the Vela pulsar at high time resolution, its absolute phase, and rotational period. We calculated for the first time an independent optical timing solution and obtained the most detailed optical pulse profile available to date. Iqueye detected a distinct narrow component on the top of one of the two main optical peaks, which was not resolved in previous observations, and a third statistically significant optical peak not aligned with the radio one. The quality of the Iqueye data allowed us to determine the relative time of arrival of the radio-optical-gamma-ray peaks with an accuracy of a fraction of a millisecond. We compare the shape of the Iqueye pulse profile with that observed in other energy bands and discuss its complex multiwavelength structure.

Key words: pulsars: general – pulsars: individual: PSR B0833−45 (Vela pulsar).

1 INTRODUCTION

The Vela pulsar (PSR J0835−4510) is one of the most intense sources in the gamma-ray and radio bands. It has a characteristic age of about 11 kyr (Lyne et al. 1996) and is located in the southern sky at a distance of 290 pc (Caraveo et al. 2001). Unlike the majority of the known pulsars, it also shows pulsed optical emission at detectable levels, with an optical magnitude of $V \sim 23.6$ (Mignani & Caraveo 2001).

PSR J0835−4510 was discovered during a survey looking for pulsars in the southern sky (Large, Vaughan & Mills 1968). It shows a periodicity of 89.3 ms and, at the time of discovery, it was the pulsar with the shortest rotational period. Large et al. (1968) noted that the pulsar was located in the centre of the Vela nebula, which has a diameter between 4° and 5°, already known to be a radio source. Compared to the Crab pulsar (see e.g. Oosterbroek et al. 2008; Germanà et al. 2012; Zampieri et al. 2014), the source is much weaker in the optical band and optical pulses were discovered only after a prolonged observing campaign using a dual photometer mounted on the Anglo-Australian telescope (Wallace et al. 1977). Later on, optical pulsations of the Vela pulsar were detected by Manchester et al. (1978), Peterson et al. (1978), Manchester et al. (1980), and Gouiffes (1998). Ultraviolet (UV) observations have been carried out with the *Hubble Space Telescope* (*HST*) by Romani, Kargaltsev & Pavlov 2005), who obtained the light curves and phase-resolved spectra in the near and far UV bands. The Vela pulsar presents also strong X-ray and gamma-ray pulsed emission with pulse profiles very different from those detected in the radio and optical bands (see e.g. Manchester & Lyne 1977; Harding et al. 2002; Abdo et al. 2009; Kuiper & Hermsen 2015). The detection of X-ray pulsations from the Vela pulsar was reported for the first time by Harnden, Johnson & Haymes (1972) and then by Harnden & Gorenstein (1973). Detailed studies of the X-ray pulse profile have been done using the data from the *ROSAT* (Oegelman, Finley & Zimmerman 1993; Seward et al. 2000), *Chandra* (Helfand, Gotthelf & Halpern 2001; Sanwal et al. 2002), *Rossi-XTE* (Strickman, Harding & de Jager 1999; Harding et al. 2002), and *XMM–Newton* (Manzali, De Luca & Caraveo 2007) telescopes. Thanks to the high time resolution of *Rossi-XTE*, Harding et al. (2002) obtained the most detailed light curve of the Vela pulsar in the X-ray band (2–30 keV) to date, finding that one of the main X-ray peaks

★ E-mail: luca.zampieri@inaf.it

© 2018 The Author(s)
Published by Oxford University Press on behalf of the Royal Astronomical Society

Downloaded from https://academic.oup.com/mnras/article/482/1/175/5106369 by Univ Degli Studi di Firenze , Biblioteca di biologia animale user on 29 March 2022

has a double structure. Later, Kuiper & Hermsen (2015) reported updated X-ray and soft gamma-ray pulse profiles. They re-analysed larger data sets from different telescopes (*XMM–Newton*, *Rossi-XTE*, *INTEGRAL*, and *COMPTEL*). Other instruments observed the Vela pulsar at gamma-ray energies (*SAS-2*, Thompson et al. 1975, 1977; *COS-B*, Bennett et al. 1977; Buccheri et al. 1978; Kanbach et al. 1980; EGRET, Kanbach et al. 1994). The latest gamma-ray studies performed with the AGILE and *Fermi*-LAT instruments (Abdo et al. 2009, 2010; Pellizzoni et al. 2009) showed the complex energy-dependent structure of the Vela pulsar light curve at GeV energies, which consists of two main peaks with a third peak and/or bridge emission in between them. Recently, Djannati-Ataï et al. (2017) reported the first detection of the pulsed emission from the Vela pulsar at 20–120 GeV with the H.E.S.S. Cherenkov telescope.

Studying optical pulsars within the framework of their multi-wavelength emission properties is crucial to improve our understanding of their emission mechanism. Multiwavelength investigations of the pulsed emission are very important for testing and constraining theoretical models describing the structure of the magnetic field and location of the pulsar emitting regions.

In this paper, we present results of the timing analysis of the Vela pulsar from the high time resolution optical observations carried out with the Iqueye instrument. Details on the observations and the data analysis procedure are reported in Section 2. Results on the timing analysis and phase folding are presented in Section 3. The discussion and conclusions follow in Section 4.

2 OBSERVATIONS AND DATA REDUCTION

In this work we analyse the observations of the Vela pulsar taken with the single photon-counting photometer Iqueye mounted at the ESO 3.5 m New Technology Telescope (NTT) in two observational runs during 2009 January (from 19 through 20) and December (from 14 through 18). Iqueye is an extremely high speed optical photon counter based on single photon avalanche photodiodes silicon detectors, which are equipped with a digital acquisition system that records arrival times of each single photon (for details see Naletto et al. 2009).

A log of the Iqueye observations of the Vela pulsar performed in two 2009 runs at NTT is reported in Table 1. Apart from a couple of very short exposures of less than 100 s, taken to test the instrument response, all the other observations have duration longer than 5 min, with most of them being above 30 min.

The data reduction is performed converting the time tags of each photon in UTC by means of a dedicated software.[1] Then, the photon arrival times are barycentred by means of the software TEMPO2, which adopts the Barycentric Coordinate Time and is accurate at the 1 ns level of precision (Edwards, Hobbs & Manchester 2006; Hobbs, Edwards & Manchester 2006).

In order to check the quality of the observations, we initially calculate light curves with bins of 1 s and inspect them. In Fig. 1 we show the light curves of the five observations with the lowest background. Obs. 4 and 14 (see Table 1) have the cleanest light curves. The total count rate measured by all four Iqueye detectors is about 1300 counts s^{-1}. Obs. 7 shows a comparatively higher background level. Obs. 12 has a good signal at the beginning but, as time goes on, the background becomes higher because of the passage of significant veils that increase the amount of scattered light. Obs. 15 has the shortest duration. The rise of the count rate towards the end of the acquisition is caused by the passage of thin clouds. As shown in Appendix A, in all these low-background-contaminated observations (Obs. 4, 7, 12, 14, and 15) we detected the pulsar signal.

[1] QUEST v. 1.1.5, Zoccarato, P. 2015, Internal Technical Report; see also Zampieri et al. (2015).

3 ANALYSIS AND RESULTS

3.1 Phase fitting of the Iqueye data

We started our analysis performing a phase fitting of the Iqueye data acquired during the 2009 December run. Following the approach already presented in Germanà et al. (2012) and Zampieri et al. (2014), we divided observations 7, 12, 14, 15 in several segments and folded them over a reference period $P_{\rm init}$. Each segment is sufficiently long (∼45 min) to detect the main peaks of the pulse profile. The reference period $P_{\rm init}$ is equal to that measured from the Iqueye data of Obs. 12 ($P_{\rm init} = 0.089\,366\,94$ s; see Appendix A). Each segment is binned with 50 bins per period.[2]

In order to determine the phase of the Vela pulsar, we fitted the two main peaks in each segment of the Iqueye pulse profile with the sum of two Gaussian functions plus a constant (see Fig. 2). The measured rotational phase ($\psi_{\rm obs}(t)$) is the mean value of the Gaussian corresponding to the second and most prominent peak. To improve the accuracy of the measurement, we fixed the separation ($\Delta\phi_{12}$) and widths (σ_1 and σ_2) of the two peaks at the following values: $\Delta\phi_{12} = 0.231$, $\sigma_1 = 0.040$, and $\sigma_2 = 0.043$. They were obtained by fitting the two main peaks of the total Iqueye pulse profile (folded using the *Fermi*-LAT timing solution; see Section 3.2) with the sum of two Gaussian functions plus a constant. The typical 1σ uncertainty on the position of the peak in each segment is 0.0071 in phase (or 0.63 ms).

The measured peak position drifts in phase because of the pulsar spin-down. The drift with respect to uniform rotation with period $P_{\rm init}$ can be written as (Germanà et al. 2012; Zampieri et al. 2014)[3]:

$$\psi(t) = \phi(t) - (t - t_0)/P_{\rm init}\,, \tag{1}$$

where t_0 is a reference time set equal to MJD 55182 and $\phi(t)$ is the phase of the pulsar peak at time t. For a 3-d baseline, the pulsar spin-down $\phi(t)$ can be reasonably well modelled with a second-order polynomial function:

$$\phi(t) = \phi_0 + \nu_0(t - t_0) + \frac{\dot{\nu}_0}{2}(t - t_0)^2, \tag{2}$$

where ϕ_0, ν_0, and $\dot{\nu}_0$ are the phase, frequency, and first frequency derivative of the pulsar at time t_0, respectively. Fitting the measured phase drift $\psi_{\rm obs}(t)$ with equations (1) and (2), we obtained the timing solution of the Iqueye December observations shown in Fig. 3 and Table 2, which is in perfect agreement with that reported in the Second *Fermi*-LAT Catalogue of Gamma-ray Pulsars (2PC; Abdo et al. 2013).

3.2 Iqueye pulse profile

The limited number of Iqueye observations (one night in January and three consecutive nights in December) does not allow us to

[2] For Obs. 7 we used 41 phase bins because of the lower signal-to-noise ratio.

[3] We note, in fact, that following Germanà et al. (2012) and Zampieri et al. (2014) $\psi(t)$ in equation (1) is defined as the opposite value of the drift.

Downloaded from https://academic.oup.com/mnras/article/482/1/175/5106369 by Univ Degli Studi di Firenze , Biblioteca di biologia animale user on 29 March 2022

Table 1. Log of the 2009 observations of the Vela pulsar taken with the Iqueye instrument at the ESO 3.5 m NTT telescope in Chile.

Obs.	Observation ID	Start time (UTC)		Start time (MJD)	Duration (s)
1	20090119-070620UTC	January 19	07:16:15.8	54850.302960	72.0
2	20090119-071240UTC	January 19	07:18:03.8	54850.304210	878.1
3	20090119-073755UTC	January 19	07:43:23.8	54850.321803	3617.0
4	20090120-052536UTC	January 20	05:31:58.3	54851.230534	7207.1
5	20091214-081325UTC	December 14	08:16:21.4	55179.344692	1264.0
6	20091216-035420UTC	December 16	04:01:03.7	55181.167403	5.0
7	20091216-040003UTC	December 16	04:03:08.7	55181.168850	7740.2
8	20091216-060939UTC	December 16	06:14:09.1	55181.259827	301.0
9	20091216-064816UTC	December 16	06:51:19.2	55181.285638	3601.0
10	20091217-034741UTC	December 17	03:51:06.7	55182.160494	301.0
11	20091217-040317UTC	December 17	04:06:44.0	55182.171342	1827.0
12	20091217-043458UTC	December 17	04:38:07.8	55182.193145	10798.8
13	20091217-073602UTC	December 17	07:39:53.3	55182.319368	2693.6
14	20091218-042650UTC	December 18	04:30:07.8	55183.187590	10798.3
15	20091218-073137UTC	December 18	07:34:48.4	55183.315835	2716.8

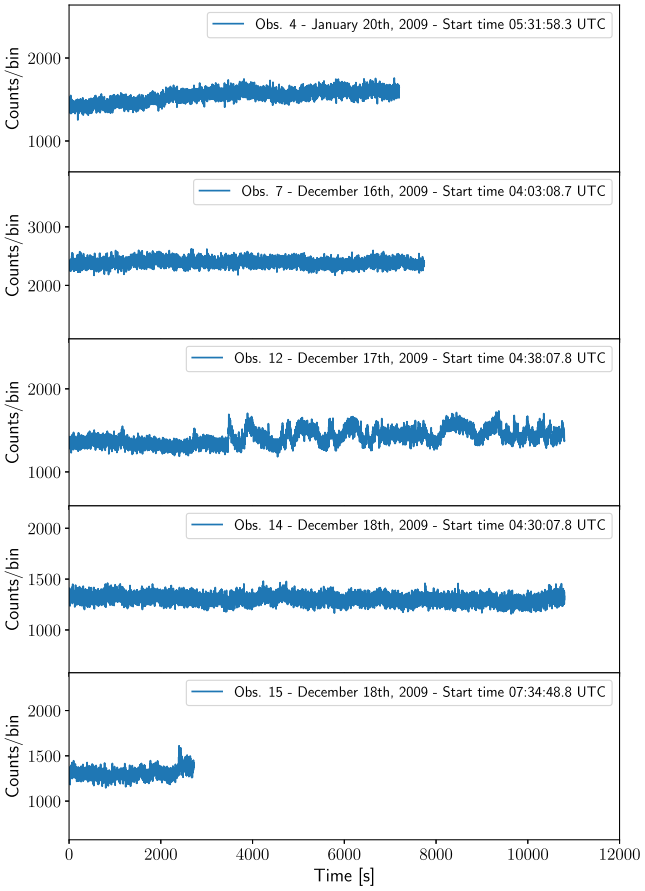

Figure 1. Light curves with time bin of 1 s of the five observations with the most significant signal (see Table 1 and the text for details).

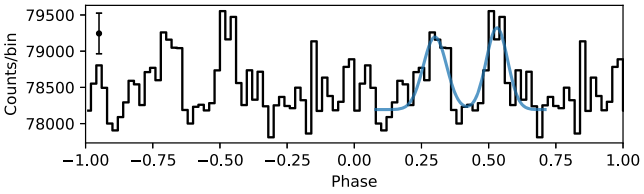

Figure 2. One of the 45 min segments of Obs. 12 folded with the period $P_{\rm init}$ =0.089 366 94 s. The blue line shows two Gaussian functions used to fit the main optical peaks. The average 1σ error bar is shown on the top left.

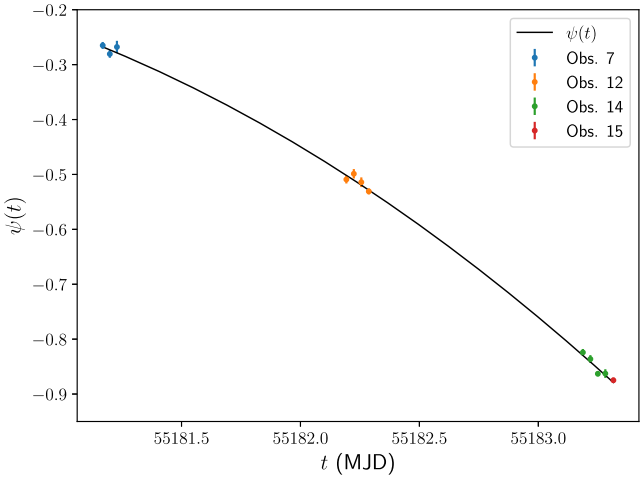

Figure 3. Phase drift of the Vela pulsar $\psi(t)$ with respect to uniform rotation. Time t expressed in MJD.

phase connect the phase of the Vela pulsar over the entire year 2009. Therefore, we folded the whole Iqueye dataset (Obs. 4, 7, 12, 14, and 15) using the accurate timing solution obtained by the *Fermi*-LAT team within the framework of the 2PC *Fermi* catalogue. The 2PC timing solution[4] is based on the rotational ephemerides computed using the 1.4 GHz radio data collected at the *Parkes* radio telescope. It covers more than 4 yr from MJD 54207.2 to MJD 55793.85 and contains 10 frequency derivatives and 15 sinusoid WAVE terms (see

[4]Available here: https://fermi.gsfc.nasa.gov/ssc/data/access/lat/ephems/

Downloaded from https://academic.oup.com/mnras/article/482/1/175/5106369 by Univ Degli Studi di Firenze , Biblioteca di biologia animale user on 29 March 2022

Table 2. Timing solution of the 2009 December run. Errors represent the 1σ statistical uncertainties.

Timing solution of the Iqueye 2009 December	
t_0	MJD 55182
ϕ_0	-0.4495 ± 0.0040
ν_0	$11.189\,816\,99 \pm 5 \times 10^{-8}$ Hz
$\dot{\nu}_0$	$(-1.35 \pm 0.13) \times 10^{-11}$ Hz^2
$P_{\rm init}$	0.089 366 94 s

Hobbs et al. 2006 for details). It also includes all the information needed to perform an absolute phase alignment with the radio pulse.

We compared the 2PC *Fermi*-LAT ephemerides with another publicly available ephemerides, which covers the dates of the Iqueye observing runs. These ephemerides have been computed using the times of arrival of the electromagnetic pulses measured with the Hobart radio telescope in Tasmania (Australia) and the Hartebeesthoek radio telescope in South Africa during the VSR2 run of the Virgo gravitational wave detector, which began on 2009 July 7 and ended on 2010 January 8 (Abadie et al. 2011). The timing solution contains two frequency derivatives. We found that it is accurate enough for performing the folding of the Iqueye data. However, the timing model from Abadie et al. (2011) has a significant difference in absolute phase (up to ∼0.4) from the 2PC timing model.

We then folded the Iqueye data with the 2PC *Fermi*-LAT ephemerides using different numbers of phase bins and found that 128 bins provide the best compromise between the error on the count rate per bin and the resolution in phase. The total folded profile was obtained summing in phase those of the single observations (Obs. 4, 7, 12, 14, and 15). The resulting pulse shape is shown in Fig. 4 and is characterized by the presence of at least four distinct peaks.

In order to obtain an accurate analytical representation of the Vela pulse profile, we fitted it with the sum of six Gaussian functions plus a constant:

$$f_{\rm opt}(\phi) = \sum_{i=1}^{6} k_i \, \frac{1}{\sqrt{2\pi}\sigma_i} \, \exp\left[-\frac{(\phi-\mu_i)^2}{2\sigma_i^2}\right] + C\,. \quad (3)$$

The values of the best-fitting parameters are listed in Table 3 170.0pt, while the resulting analytical template is shown in Fig. 4. The reduced χ^2 of the fit is 0.977. Three of the peaks in the pulse profile (P1s, P3, and P4) are fitted with single Gaussians centred at phases 0.256, 0.841, 1.0, respectively. Peak P2s at phase ∼0.47 is fitted with the sum of two Gaussian components (P2s-1 and P2s-2). Another broad Gaussian at phase 0.56 is required to reproduce the complex background.

To estimate the significance of the various peaks we compared the best-fitting model $f_{\rm opt}$ with one in which the amplitude of each component was reduced by a factor of 5. We computed the *F*-statistics and the corresponding probability by comparing the χ^2 of the fits with these two models, obtaining the significance of each component in Gaussian sigmas. For the two prominent peaks P1s and P2s the significance is clearly very high, while that of peaks P3 and P4 is 3.9σ and 5.5σ, respectively. We also estimated that the significance of the narrower peak P2s-1 at phase 0.451 is 5.7σ.

In order to double check the robustness of our results, we repeated all the analysis folding the pulse profiles using 64 bins in phase and obtained similar results (the significance of peaks P2s-1, P3, and P4 is 5.1σ, 3.6σ, and 4.8σ, respectively).

3.3 *Fermi*-LAT pulse profile

To perform an accurate comparison of the phase of the optical peaks to that at other wavelengths, we used as reference the gamma rays. We then analysed the *Fermi*-LAT data with the *Fermi*Science Tools software package v11r5p3,[5] and obtained the high-energy pulse profile of the Vela pulsar using a technique similar to one described in Section 3.2.

We used more than 3 yr of available data accumulated by the *Fermi*satellite during the time interval from MJD 54682.66 to MJD 55793.85, fully covered by the 2PC timing solution. We extracted events with energies between 30 MeV and 300 GeV. To improve the signal to noise ratio we used an energy-dependent extraction region selecting only events within an angle $\theta < \max\,[1.6 - 3\log_{10}(E_{\rm GeV}), 1.3]$ deg from the Vela pulsar position,[6] where $E_{\rm GeV}$ is the energy of the event measured in GeV (see Abdo et al. 2009, 2010). We excluded events detected during the periods when the Vela pulsar is viewed at zenith angles >90° in order to minimize the contamination from the Earth limb. After selecting the events and determining the good time intervals of the *Fermi*-LAT data we performed a barycentric correction of the photon arrival times using the tool `gtbary`.

We calculated the phase of each photon and folded the *Fermi*-LAT data using the 2PC timing solution. The final gamma-ray pulse profile of the Vela pulsar is shown in Fig. 4. As for the Iqueye profile, we used 128 phase bins. We then fitted the gamma-ray pulse profile with an analytical function f_γ which is the sum of tree Gaussians, a lognormal function and a constant[7]:

$$f_\gamma(\phi) = \sum_{i=1}^{3} k_i \, \frac{1}{\sqrt{2\pi}\sigma_i} \, \exp\left[-\frac{(\phi-\mu_i)^2}{2\sigma_i^2}\right] + k_4 \, \frac{1}{(\phi-\phi_0)\sqrt{2\pi}\sigma_4} \, \exp\left[-\frac{(\ln(\phi-\phi_0)-\mu_4)^2}{2\sigma_4^2}\right] + C\,. \quad (4)$$

The best-fitting values of the parameters are listed in Table 4. The reduced χ^2 value of the fit is rather high (16.4) because of the small error bars of the *Fermi*-LAT profile. However, the two main gamma-ray peaks P1h and P2h are well reproduced for our purposes.

3.4 Relative timing of the radio-optical-gamma-ray peaks

As the Iqueye pulse profile contains multiple overlapping components, we determined the centroid of each peak calculating the local maxima of the function $f_{\rm opt}$. To this end, we computed the zeros of the derivative f'_{opt} ($\equiv df_{opt}/d\phi$). Uncertainties of the peak positions were estimated from the difference of the zeros of the functions $f'_{\rm opt} + \delta f'_{\rm opt}$ and $f'_{\rm opt} - \delta f'_{\rm opt}$, where $\delta f'_{\rm opt}$ is obtained propagating

[5] https://fermi.gsfc.nasa.gov/ssc/data/analysis/software/.

[6] The equatorial coordinates of the Vela pulsar are taken from the 2PC ephemerides: $\alpha = 128.835\,839\,242°$, $\delta = -45.176\,336\,389°$.

[7] We used Gaussian components to fit the gamma-ray peaks and not asymmetric Lorentzian functions (as e.g. in Abdo et al. 2010) to avoid additional systematic uncertainties when comparing the Iqueye and *Fermi*-LAT peaks profiles. We also tried to replace the lognormal component with a fourth Gaussian function, but it worsened the fit.

Downloaded from https://academic.oup.com/mnras/article/482/1/175/5106369 by Univ Degli Studi di Firenze , Biblioteca di biologia animale user on 29 March 2022

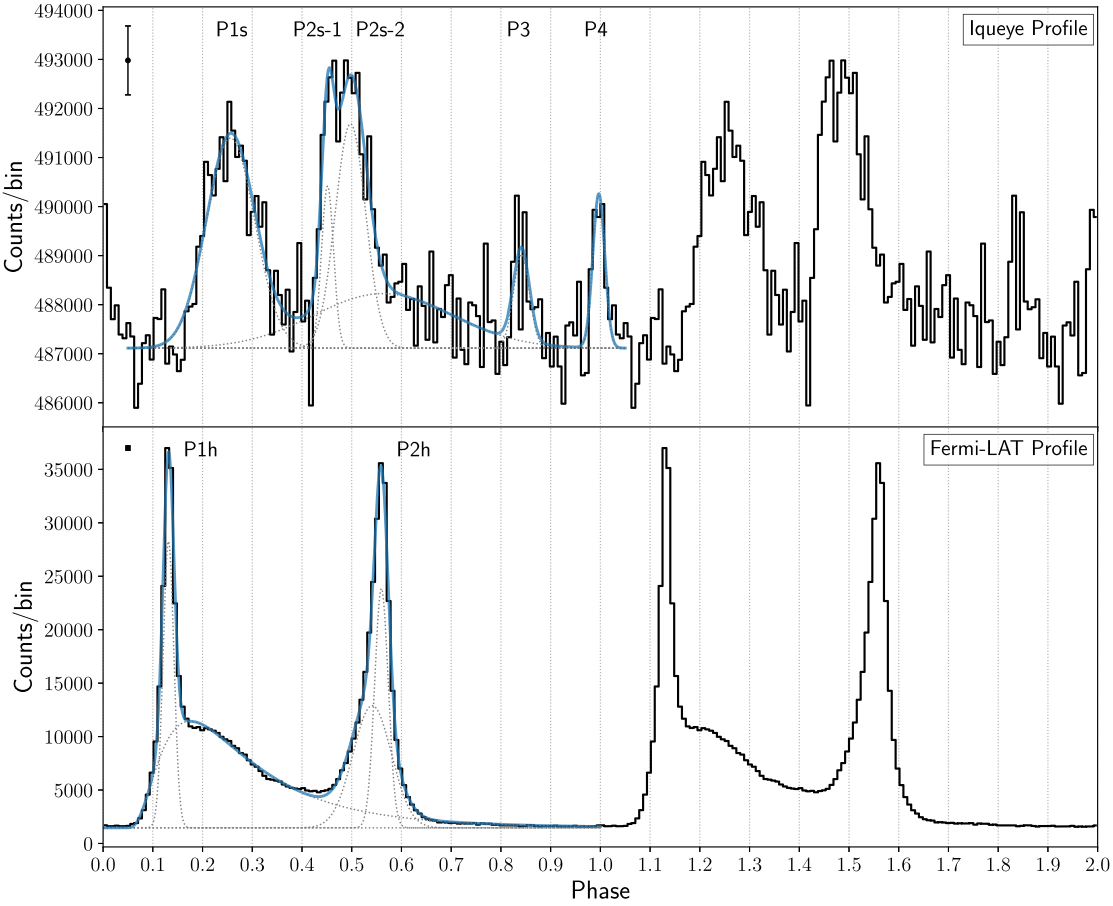

Figure 4. Two periods of the Vela pulsar pulse profile from the Iqueye optical observations taken in 2009 (*top panel*) and the *Fermi*-LAT gamma-ray observations taken during 3 yr of its operation (MJD 54682.66–55793.85, *bottom panel*). The blue line in each plot shows the best-fitting analytical function which reproduces the profile. Individual components of these functions are also shown with grey dashed lines. Phase 0 corresponds to the radio peak. The average 1σ error bar is shown on the top left.

Table 3. Best-fitting parameters of function $f_{\rm opt}$ (equation 3) adopted to fit the Iqueye pulse profile of the Vela pulsar. Errors represent the 1σ statistical uncertainties.

i	μ_i	σ_i	k_i
1	0.256 ± 0.004	0.049 ± 0.004	520 ± 50
2	0.451 ± 0.003	0.012 ± 0.004	100 ± 60
3	0.497 ± 0.007	0.031 ± 0.007	350 ± 90
4	0.56 ± 0.04	0.14 ± 0.04	400 ± 100
5	0.841 ± 0.004	0.016 ± 0.005	80 ± 20
6	1.000 ± 0.002	0.012 ± 0.002	90 ± 20
$C = 487100 \pm 200$			

Table 4. Best-fitting parameters of the function f_γ (equation 4) adopted to fit the *Fermi*-LAT pulse profile of the Vela pulsar. Errors represent the 1σ statistical uncertainties.

i	μ_i	σ_i	k_i	ϕ_0
1	0.1315 ± 0.0002	0.0109 ± 0.0002	730 ± 20	–
2	0.5411 ± 0.0009	0.0387 ± 0.0008	1110 ± 30	–
3	0.5597 ± 0.0003	0.0137 ± 0.0004	770 ± 30	–
4	$\ln(0.208 \pm 0.004)$	0.66 ± 0.02	2770 ± 60	0.040 ± 0.004
$C = 1460 \pm 40$				

the errors of the fitted parameters p_i on $f'_{\rm opt}$:

$$\delta f'_{\rm opt} = \sqrt{\sum_i \sum_j \left(\frac{\partial f'_{\rm opt}}{\partial p_i}\right)\left(\frac{\partial f'_{\rm opt}}{\partial p_j}\right)\sigma_{ij}}. \quad (5)$$

σ_{ij} are elements of the covariance matrix of the fit. The final positions of the peaks of the Iqueye optical pulse profile determined in this way are listed in Table 5. The positions of the peaks P1h and P2h of the *Fermi*-LAT gamma-ray pulse profile and their corresponding uncertainties have been calculated in the same way and are also listed in Table 5.

The quality of the Iqueye pulse shape allows us to determine the relative time shift between the narrower optical and gamma-ray/radio peaks with an accuracy of a fraction of a millisecond. The gamma-ray peak P1h is leading the optical peak P1s by 0.125 ± 0.004 (11.2 ± 0.4 ms). The high-energy peak P2h is trailing both optical peaks P2s-1 and P2s-2 by $0.104^{+0.005}_{-0.003}$ and $0.061^{+0.003}_{-0.007}$, respectively. Peak P3 is leading the radio peak by 0.159 ± 0.005 (14.2 ± 0.4 ms), whereas peak P4 turns out to be aligned in phase with the radio peak within the 3σ errors.

The dominant source of the uncertainties are fitting errors on the parameters of the functions $f_{\rm opt}$ and f_γ. The broadening of the peaks caused by uncertainties of the 2PC *Fermi*-LAT timing solution has a small influence. To confirm this we folded both the Iqueye and

Downloaded from https://academic.oup.com/mnras/article/482/1/175/5106369 by Univ Degli Studi di Firenze , Biblioteca di biologia animale user on 29 March 2022

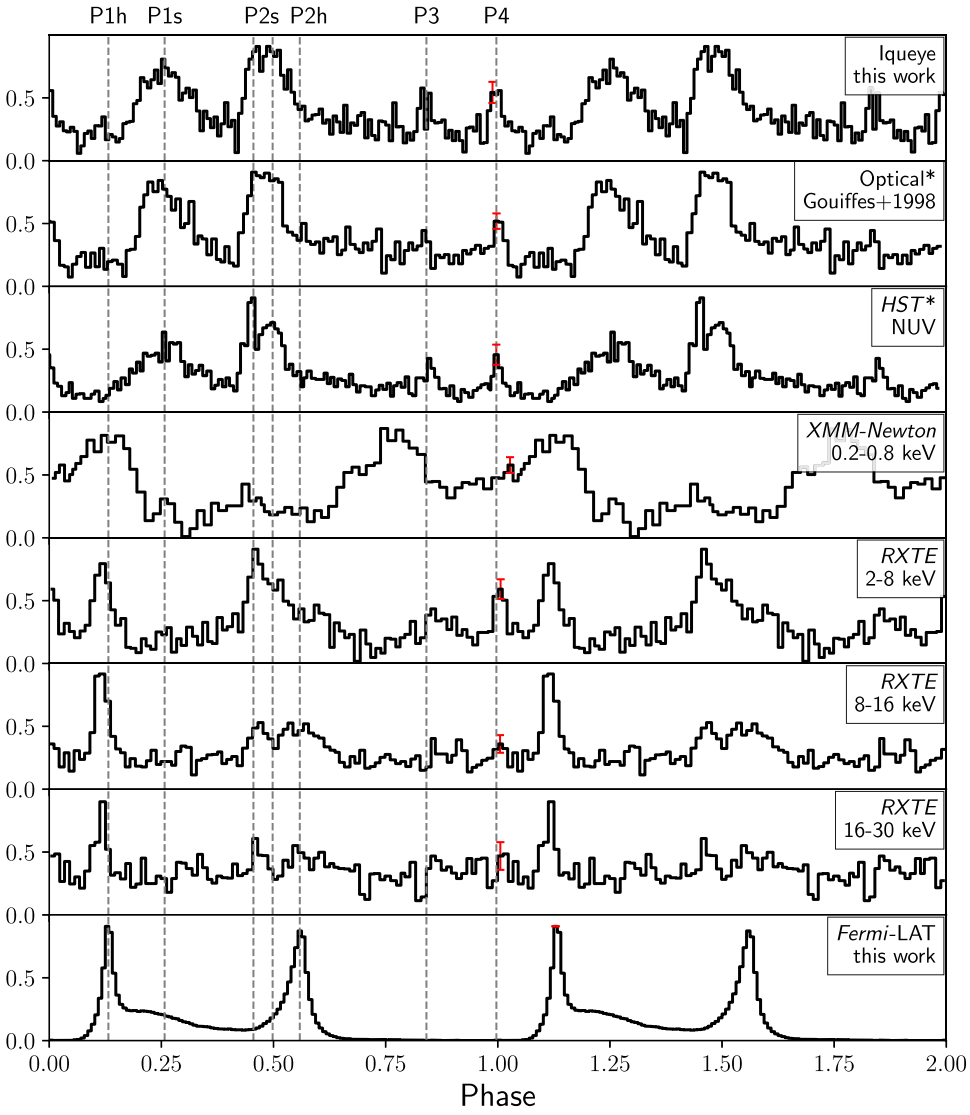

Figure 5. Normalized pulse profiles of the Vela pulsar in different energy bands. Optical, near UV, and X-ray profiles are adopted from Gouiffes (1998), Romani et al. (2005), and Kuiper & Hermsen (2015) and Harding et al. (2002), respectively. Pulse profiles from Gouiffes (1998) and Romani et al. (2005) (marked with asterisks) are shifted so as to align them with the Iqueye profile (see the text for details). Phase 0 corresponds to the radio peak. The vertical dotted lines mark the positions of different peaks. The average 1σ error bar for each profile is shown in red.

Table 5. Peak positions of the Iqueye and *Fermi*-LAT pulse profiles. Errors represent the estimated 1σ statistical uncertainties (see the text for details).

Iqueye pulse profile	
P1s	0.257 ± 0.004
P2s-1	$0.455^{+0.005}_{-0.003}$
P2s-2	$0.498^{+0.004}_{-0.007}$
P3	0.841 ± 0.005
P4	0.997 ± 0.002
Fermi-LAT pulse profile	
P1h	0.1319 ± 0.0002
P2h	0.5586 ± 0.0003

Fermi-LAT data with two timing solutions that, considering the uncertainties on the 2PC ephemerides, extremize the deviations from the mean timing solution. The differences between the peak positions determined by means of these two timing solutions are smaller than corresponding fitting errors and, therefore, can be neglected.

4 DISCUSSION AND CONCLUSIONS

The aim of this work is to present the analysis of the optical data of the Vela pulsar obtained with the Iqueye instrument at the ESO NTT telescope. The observations collected with Iqueye were used to produce for the first time an independent optical timing solution. We also obtained the most detailed optical pulse profile of the Vela pulsar available to date.

The pulse shape of the Vela pulsar detected with Iqueye has a better resolution and shows a finer structure than those obtained in previous optical investigations (e.g. Manchester et al. 1980; Gouiffes

Downloaded from https://academic.oup.com/mnras/article/482/1/175/5106369 by Univ Degli Studi di Firenze , Biblioteca di biologia animale user on 29 March 2022

1998). It shows new features such as the double-peak structure of peak P2s and a significant peak P3, that were not clearly identified in the optical band before. The overall quality of the profile is comparable to that obtained in the UV band by Romani et al. (2005) using the *HST*STIS (Space Telescope Imaging Spectrograph).

We determined the phase of each optical peak with an accuracy of a fraction of a millisecond relative to the peaks in the radio and gamma-ray bands. Such accurate measurements can be used in the future for testing theoretical models which describe the location of the pulsar emitting regions. Here we simply note that, although within the formal errors the two peaks are aligned, in fact there is some hint that the optical peak P4 may be leading the radio one by a few hundred microseconds (0.003 in phase). This would be perfectly consistent with the shift measured in the Crab pulsar (Zampieri et al. 2014).

In Fig. 5 we compare the shape of the Iqueye and *Fermi*-LAT pulse profiles obtained here with those at other wavelengths. The optical, UV and X-ray profiles are taken from Gouiffes (1998), Romani et al. (2005), and Harding et al. (2002) and Kuiper & Hermsen (2015), respectively. As the accuracy on the absolute phase measurement of Gouiffes (1998) is not known and the absolute timing precision of the *HST*STIS data in Romani et al. (2005) is limited to 10 ms, in Fig. 5 we shifted the corresponding pulse profiles as to align them with the more accurate profile obtained with Iqueye.[8]

The multiwavelength pulse profile of the Vela pulsar shows at least five components. Starting from phase zero, at the radio peak, and moving to larger phases, we see first some emission at low energies which is difficult to disentangle from that of the underlying background. Then, at phase ∼0.1, the line of sight suddenly enters in the narrow bright gamma-ray peak P1h emission region, where X-ray emission is also significant (Harding et al. 2002; Kuiper & Hermsen 2015) and optical emission is only marginal. At larger phases, the line of sight passes through the optical peaks P1s and P2s. Peak P2s is well structured in the optical and UV bands. There is a narrow peak on its edge (denoted as P2s-1), which is aligned with one in the X-rays. In gamma-rays we see a region of continuous moderate bridge emission, which changes morphology with increasing energy (Abdo et al. 2009, 2010). This region terminates sharply at phase 0.6, where the second gamma-ray/X-ray peak P2h is located. From phase 0.6 through phase 1, gamma-ray emission is not present and no other prominent emission features are visible in the other spectral bands, with the exception of peak P3 and a broad soft X-ray peak at phase 0.8 (whose tail extends up to peak P1h, forming a sort of bridge emission, Kuiper & Hermsen 2015). At phase 1.0 the line of sight crosses the radio peak, which is aligned with peak P4 visible in the optical, UV, and X-ray bands.

We suggest that the optical emission originates from three different regions: optical peaks P1s and P2s-1 are likely to originate near the X-ray and gamma-ray emission regions, whereas optical peaks P3 and P4 may form closer to the soft X-ray and radio emission regions, respectively. The optical/hard X-ray/gamma-ray emission region may be located along magnetic field lines originating from a single magnetic pole (Manchester & Lyne 1977; Manchester et al. 1980) or neighbouring magnetic field lines, while the radio/optical and soft X-ray/optical emission originate far from them. Indeed, none of main X-ray/gamma-ray peaks is in phase with the radio peak at phase 0. Such a complex emission pattern could be produced by electrons accelerated to higher and higher energies as they travel along a bundle of field lines that opens more and more farther out in the pulsar magnetosphere. This scenario is consistent with models that favour a high-altitude origin of the gamma-ray emission (see e.g. Romani & Yadigaroglu 1995; Bai & Spitkovsky 2010a,b; Rudak & Dyks 2017).

Future optical observations could allow us to achieve even better statistics in determining the pulse profile of the Vela pulsar and its fine structure, which turns out to be possible only for a handful of pulsars. This is needed to complement the information from other high energy bands and improve our understanding of the complex emission and magnetic field geometry of the Vela pulsar.

[8]This shift was calculated from the average of the difference between the position of the Iqueye optical peaks P1s, P2s-1, P2s-2, P3, and P4 (Table 5) and that of the Gouiffes (1998) and Romani et al. (2005) pulse profiles, the latter obtained by fitting each peak with a Gaussian function.

ACKNOWLEDGEMENTS

We would like to thank an anonymous referee for his/her constructive and insightful comments that helped us improving the paper. We also thank Tommaso Occhipinti, Ivan Capraro, Andrea di Paola, and Paolo Zoccarato for their crucial contribution to the development of the acquisition system of Iqueye and for their support with the observations and data collection at the telescope. AP acknowledges support from a Netherlands Organization for Scientific Research (NWO) Vidi fellowship. This work is based on observations made with the ESO NTT telescope at the La Silla Paranal Observatory under programmes IDs 082.D-0382 and 084.D-0328(A). This research has been partly supported by the University of Padova under the Quantum Future Strategic Project, by the Italian Ministry of University MIUR through the programme PRIN 2006, by the Project of Excellence 2006 Fondazione CARIPARO, and by INAF-Astronomical Observatory of Padova. This research made use also of the following PYTHON packages: MATPLOTLIB (Hunter 2007)),NUMPY (van der Walt et al. 2011), and ASTROPY (Astropy Collaboration et al. 2013).

REFERENCES

Abadie J. et al., 2011, ApJ, 737, 93
Abdo A. A. et al., 2009, ApJ, 696, 1084
Abdo A. A. et al., 2010, ApJ, 713, 154
Abdo A. A. et al., 2013, ApJS, 208, 17
Astropy Collaboration et al., 2009, ApJ, 697, 1071
Bai X.-N., Spitkovsky A., 2010a, ApJ, 715, 1270
Bai X.-N., Spitkovsky A., 2010b, ApJ, 715, 1282
Bennett K. et al., 1977, A&A, 61, 279
Buccheri R. et al., 1978, A&A, 69, 141
Caraveo P. A., De Luca A., Mignani R. P., Bignami G. F., 2001, ApJ, 561, 930
Djannati-Ataï A., Giavitto G., Holler M., Rudak B., Venter C., 2017, in Aharonian F. A., Hofmann W., Rieger F. M., eds, AIP Conf. Proc. Vol. 1792, 6th International Meeting on High Energy Gamma-Ray Astronomy, p. 040028
Edwards R. T., Hobbs G. B., Manchester R. N., 2006, MNRAS, 372, 1549
Germanà C. et al., 2012, A&A, 548, A47
Gouiffes C., 1998, in Shibazaki N. et al., eds, Neutron Stars and Pulsars: Thirty Years after the Discovery, Universal Academy Press, Tokyo, Japan,p. 363
Harding A. K., Strickman M. S., Gwinn C., Dodson R., Moffet D., McCulloch P., 2002, ApJ, 576, 376
Harnden F. R., Gorenstein P., 1973, Nature, 241, 107

Downloaded from https://academic.oup.com/mnras/article/482/1/175/5106369 by Univ Degli Studi di Firenze , Biblioteca di biologia animale user on 29 March 2022

Harnden F. R., Jr., Johnson W. N., III, Haymes R. C., 1972, ApJ, 172, L91
Helfand D. J., Gotthelf E. V., Halpern J. P., 2001, ApJ, 556, 380
Hobbs G. B., Edwards R. T., Manchester R. N., 2006, MNRAS, 369, 655
Hunter J. D., 2007, Comput. Sci. Eng., 9, 90
Kanbach G. et al., 1980, A&A, 90, 163
Kanbach G. et al., 1994, A&A, 289, 855
Kuiper L., Hermsen W., 2015, MNRAS, 449, 3827
Large M. I., Vaughan A. E., Mills B. Y., 1968, Nature, 220, 340
Leahy D. A., Darbro W., Elsner R. F., Weisskopf M. C., Kahn S., Sutherland P. G., Grindlay J. E., 1983, ApJ, 266, 160
Lyne A. G., Pritchard R. S., Graham-Smith F., Camilo F., 1996, Nature, 381, 497
Manchester R. N., Lyne A. G., 1977, MNRAS, 181, 761
Manchester R. N., Wallace P. T., Peterson B. A., Elliott K. H., 1980, MNRAS, 190, 9P
Manchester R. N. et al., 1978, MNRAS, 184, 159
Manzali A., De Luca A., Caraveo P. A., 2007, ApJ, 669, 570
Mignani R. P., Caraveo P. A., 2001, A&A, 376, 213
Naletto G. et al., 2009, A&A, 508, 531
Oegelman H., Finley J. P., Zimmerman H. U., 1993, Nature, 361, 136
Oosterbroek T. et al., 2008, A&A, 488, 271
Pellizzoni A. et al., 2009, ApJ, 691, 1618
Peterson B. A., Murdin P., Wallace P., Manchester R. N., Penny A. J., Jorden A., Hartley K. F., King D., 1978, Nature, 276, 475
Romani R. W., Kargaltsev O., Pavlov G. G., 2005, ApJ, 627, 383
Romani R. W., Yadigaroglu I.-A., 1995, ApJ, 438, 314
Rudak B., Dyks J., 2017, preprint (arXiv:1708.01556)
Sanwal D., Pavlov G. G., Kargaltsev O. Y., Garmire G. P., Zavlin V. E., Burwitz V., Manchester R. N., Dodson R., 2002, in Slane P. O., Gaensler B. M., eds, ASP Conf. Ser. Vol. 271, Neutron Stars in Supernova Remnants. Astron. Soc. Pac., San Francisco, p. 353
Seward F. D., Alpar M. A., Flanagan C., Kızıloğlu Ü., Markwardt C., McCulloch P., Ögelman H., 2000, ApJ, 536, 948
Stella L., Angelini L., 1992, in di Gesu V., Scarsi L., Buccheri R., Crane P., eds, Data Analysis in Astronomy, Plenum Press, New York. p. 59
Strickman M. S., Harding A. K., de Jager O. C., 1999, ApJ, 524, 373
Thompson D. J., Fichtel C. E., Kniffen D. A., Ogelman H. B., 1975, ApJ, 200, L79
Thompson D. J., Fichtel C. E., Kniffen D. A., Ogelman H. B., 1977, ApJ, 214, L17
van der Walt S. et al., 2011, Comput. Sci. Eng., 13, 22
Wallace P. T. et al., 1977, Nature, 266, 692
Zampieri L. et al., 2014, MNRAS, 439, 2813
Zampieri L. et al., 2015, in Prochazka I., Sobolewski R., James R. B., eds, Proc. SPIE Conf. Ser. Vol. 9504, Photon Counting Applications. SPIE, Bellingham, p. 95040C

APPENDIX A: VELA PULSAR PERIOD SEARCH IN THE IQUEYE DATA

We carried out an independent search for pulsations on the optical data to test the sensitivity and accuracy of our instrument to the pulsar signal. We then calculated power density spectra (PDS) of all light curves using different time bins (from 1 to 10 ms) with the XRONOS task `powspec` (Stella & Angelini 1992). The time bin was varied in order to identify possible spurious low-significance peaks induced by the noise. The PDS are Leahy normalized (Leahy et al. 1983). For an optimal detection of periodic signals we computed a single PDS for the entire length of each observation (frequency resolution $\approx 10^{-4}$ Hz).

One observation (Obs. 14) shows a clear peak at a significance $\sim 9\sigma$ single trial (7σ for 539 915 independent trials) in the power spectrum (see Fig. A1). The frequency of this peak is 11.1898 Hz. Other two observations show peaks at 11.1898 Hz with a significance of $\sim 6\sigma$ single trial (Obs. 12 and 15).

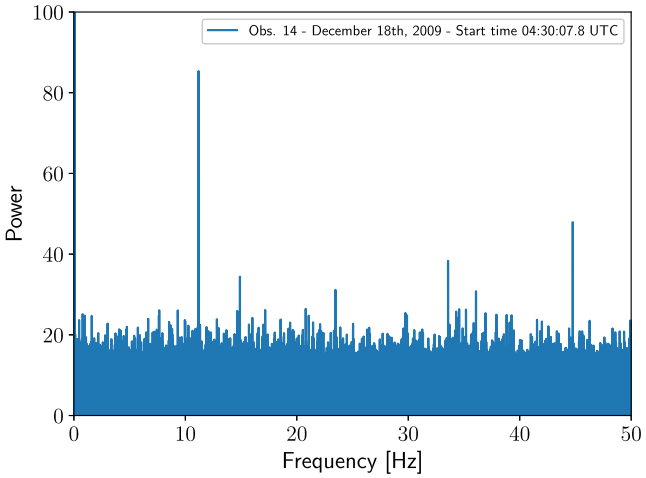

Figure A1. Leahy normalized power spectrum of Obs. 14 (see Table 1). The time bin is 0.01 s. The resolution in frequency is 10^{-4} Hz.

Table A1. Periods of the Vela pulsar obtained with Iqueye. Data are barycentred in `TEMPO2` mode. The last digit in brackets is the 1σ statistical error.

Obs.	Start time (MJD)	Frequency (Hz)	Period (s)	$\chi^2_{\max}$ [a]
4	54851.230534	11.190 33(5)	0.089 362 89(4)	190
7	55181.168850	11.189 82(3)	0.089 366 95(2)	240
12	55182.193145	11.189 82(1)	0.089 366 94(8)	379
14	55183.187590	11.189 82(1)	0.089 366 98(9)	468
15	55183.315835	11.189 80(3)	0.089 367 10(2)	279

[a]Maximum value of the χ^2 reported in Fig. A2.

The peak at the lowest frequency corresponds to the fundamental frequency associated with the rotation of the pulsar and provides its period of rotation, $p = 1/\nu = 0.089\,367$ s. Interestingly, the frequencies at 33.5694 and 44.7592 Hz detected in the power spectrum of Obs. 14 correspond to the third and fourth harmonics of the fundamental and are present (though not always) also when varying the time bin. Furthermore, as it can be seen in the optical pulse profile, the distance in phase between the two main peaks is approximately 1/4 in phase, which is consistent with the presence of a significant fourth harmonic component in the power spectrum.

We then performed a refined search with the folding technique using the task `efsearch` in XRONOS. The final rotational periods obtained for these observations (Obs. 12, 14, and 15) and the maximum values of the χ^2 are reported in Table A1 (for data barycentred with TEMPO2). The corresponding χ^2 curves are shown in Fig. A2. The error on the rotational period was estimated by fitting the peak of the distribution of the χ^2 with a Gaussian.[9] The dispersion of the

[9]The time resolution for the period search is <100 ns. For larger resolutions the peak is not sufficiently well defined.

Downloaded from https://academic.oup.com/mnras/article/482/1/175/5106369 by Univ Degli Studi di Firenze , Biblioteca di biologia animale user on 29 March 2022

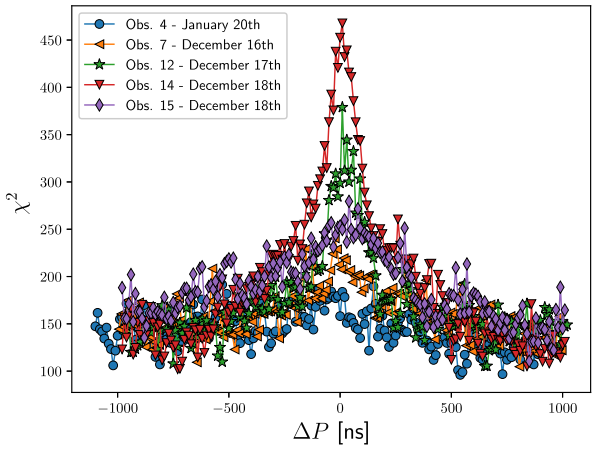

Figure A2. Distribution of the χ^2 for the Vela pulsar light curves, folded with different rotational periods. Each curve is shifted with the corresponding value of the rotational period reported in Table A1. Data are barycentred in TEMPO2 mode.

Gaussian provides a conservative estimate of the error, which turns out to be ∼20 ns.

We used the 2PC *Fermi*-LAT ephemerides to search for pulsations in the optical observations with no significant signal in the power spectrum, including those taken in January. The folding technique allowed us to find a weak signal in other two observations, Obs. 4 in January and Obs. 7 in December. The corresponding rotational periods and χ^2 curves are also shown in Table A1 and Fig. A2.

This paper has been typeset from a TEX/LATEX file prepared by the author.

Downloaded from https://academic.oup.com/mnras/article/482/1/175/5106369 by Univ Degli Studi di Firenze , Biblioteca di biologia animale user on 29 March 2022